Spinocerebellar ataxia type 6 knockin mice develop a progressive neuronal dysfunction with age-dependent accumulation of mutant $Ca_V2.1$ channels

Kei Watase*†‡, Curtis F. Barrett§¶, Taisuke Miyazaki‖, Taro Ishiguro*, Kinya Ishikawa*, Yuanxin Hu**, Toshinori Unno*, Yaling Sun†, Sayumi Kasai*, Masahiko Watanabe‖, Christopher M. Gomez**, Hidehiro Mizusawa*, Richard W. Tsien§, and Huda Y. Zoghbi†‡††

*Twenty-First Century Center of Excellence Program on Brain Integration and Its Disorders, Tokyo Medical and Dental University, 1-5-45 Yushima, Bunkyo-ku, Tokyo 113-8519, Japan; †Department of Molecular and Human Genetics, ‡Howard Hughes Medical Institute, Baylor College of Medicine, One Baylor Plaza, Houston, TX 77030; §Department of Molecular and Cellular Physiology, Stanford University School of Medicine, Stanford, CA 94305; ‖Department of Anatomy, Hokkaido University School of Medicine, Sapporo 060-8638, Japan; and **Department of Neurology, University of Chicago, 5841 South Maryland Avenue, Chicago, IL 60637

Contributed by Huda Y. Zoghbi, May 5, 2008 (sent for review March 6, 2008)

Spinocerebellar ataxia type 6 (SCA6) is a neurodegenerative disorder caused by CAG repeat expansions within the voltage-gated calcium (Ca_V) 2.1 channel gene. It remains controversial whether the mutation exerts neurotoxicity by changing the function of $Ca_V2.1$ channel or through a gain-of-function mechanism associated with accumulation of the expanded polyglutamine protein. We generated three strains of knockin (KI) mice carrying normal, expanded, or hyperexpanded CAG repeat tracts in the *Cacna1a* locus. The mice expressing hyperexpanded polyglutamine (*Sca6*^{84Q}) developed progressive motor impairment and aggregation of mutant $Ca_V2.1$ channels. Electrophysiological analysis of cerebellar Purkinje cells revealed similar Ca^{2+} channel current density among the three KI models. Neither voltage sensitivity of activation nor inactivation was altered in the *Sca6*^{84Q} neurons, suggesting that expanded CAG repeat *per se* does not affect the intrinsic electrophysiological properties of the channels. The pathogenesis of SCA6 is apparently linked to an age-dependent process accompanied by accumulation of mutant $Ca_V2.1$ channels.

cerebellum | polyglutamine | P/Q-type voltage-dependent calcium channel

Spinocerebellar ataxia type 6 (SCA6) is one of nine known dominantly inherited neurodegenerative disorders caused by the expansion of a CAG repeat. In SCA6, the CAG repeat encodes a polyglutamine tract in the $Ca_V2.1$ voltage-gated calcium channel subunit (*CACNA1A*) (1). The *CACNA1A* gene undergoes alternative splicing such that one splice variant translates the polyglutamine tract from a CAG repeat tract residing in the last coding exon (exon 47). Although $Ca_V2.1$ is expressed widely in brain, the mutation causes degeneration of cerebellar Purkinje cells (PCs) and inferior olivary neurons (2, 3).

The pathogenesis of polyglutamine diseases is quite complex in that the different proteins have diverse functions, but the diseases are all caused by an apparent gain-of-function pathogenic mechanism (4). Some features unique to SCA6 set it apart from other polyglutamine diseases. First, the disease arises from a relatively small expansion, with as few as 19 repeats (1, 5) compared with other polyglutamine diseases in which 35–300 repeats cause disease. Second, the CAG tract is present in an alternatively spliced exon, whereas in other disorders the repeat is translated in all isoforms.

The $Ca_V2.1$ subunit encodes P/Q-type voltage-sensitive Ca^{2+} channels, which play a critical role in neurotransmitter release (6) and generation of precise intrinsic pace making in PCs (7). Thus, it is quite logical to anticipate that the CAG repeat expansions would affect this particular function of the channel. Surprisingly, however, the data available so far do not provide conclusive evidence as to whether the small CAG repeat expansions cause disease by altering the function or expression of $Ca_V2.1$ channel currents (8–11). A major limitation to data interpretation is that all previous studies have relied on overexpression models in a heterologous system. Thus, it is critical to study the consequences of glutamine-expanded $Ca_V2.1$ channels when they are expressed in their endogenous neuronal environment at physiologically relevant levels.

To model SCA6 in mice, we used gene targeting to generate three lines (*Sca6*^{14Q}, *Sca6*^{30Q}, and *Sca6*^{84Q}) of knockin (KI) mouse models, carrying either 14 (normal human allele), 30 (expanded SCA6 allele), or 84 (hyperexpanded allele) CAG repeats in the mouse *Cacna1a* locus. Investigating the function of the $Ca_V2.1$ channel in all three SCA6 KI mice allowed us to gain insight about how posttranscriptional regulation might impact channel function and the likely mechanisms mediating SCA6 pathogenesis.

Results

Generation of Sca6 KI Mice. Mouse *Cacna1a* is highly homologous to human *CACNA1A*; however, mouse exon 47 lacks both the CAG repeat tract and its flanking sequence [supporting information (SI) Fig. S1*C*]. At the boundary of mouse intron 46/exon 47, we confirmed the presence of the sequence AGGGCAGTAG, in which each of the three AG sequences can serve as a splice acceptor site to generate distinct isoforms (12) (Fig. S1 *A* and *B*). Splicing to the first AG results in an isoform with a long C-terminal tail (termed the MPI isoform), whereas splicing to the second site produces a short C terminus (MPc) caused by the introduction of a stop codon. Splicing to the third AG site gives rise to a rare isoform (MPII) in mouse PCs. We introduced the CAG repeat and its immediate flanking sequence derived from *CACNA1A* into the *Cacna1a* locus by using homologous recombination in embryonic stem (ES) cells derived from 129/SvEv strain (Fig. 1*A*; see *Methods* for details). Germ-line transmission of the targeted allele in the offspring was confirmed by Southern blot analysis (Fig. 1*B* and data not shown). To verify expression of the mutant transcripts, we performed RT-PCR analysis with primers designed to amplify the CAG repeat tract and its flanking human sequence. As shown in Fig. S2*A*, the bands of expected size were present in amplified cDNA from KI alleles.

Author contributions: K.W., M.W., H.M., R.W.T., and H.Y.Z. designed research; K.W., C.F.B., T.M., T.I., K.I., T.U., Y.S., and S.K. performed research; Y.H. and C.M.G. contributed new reagents/analytic tools; K.W., T.M., K.I., and H.Y.Z. analyzed data; and K.W., C.F.B., T.M., and H.Y.Z. wrote the paper.

The authors declare no conflict of interest.

Freely available online through the PNAS open access option.

¶Present address: Neurology and Human Genetics, Leiden University Medical Centre, Albinusdreef 2, 2333 ZA, Leiden, The Netherlands.

††To whom correspondence should be addressed. E-mail: hzoghbi@bcm.tmc.edu.

This article contains supporting information online at www.pnas.org/cgi/content/full/0804350105/DCSupplemental.

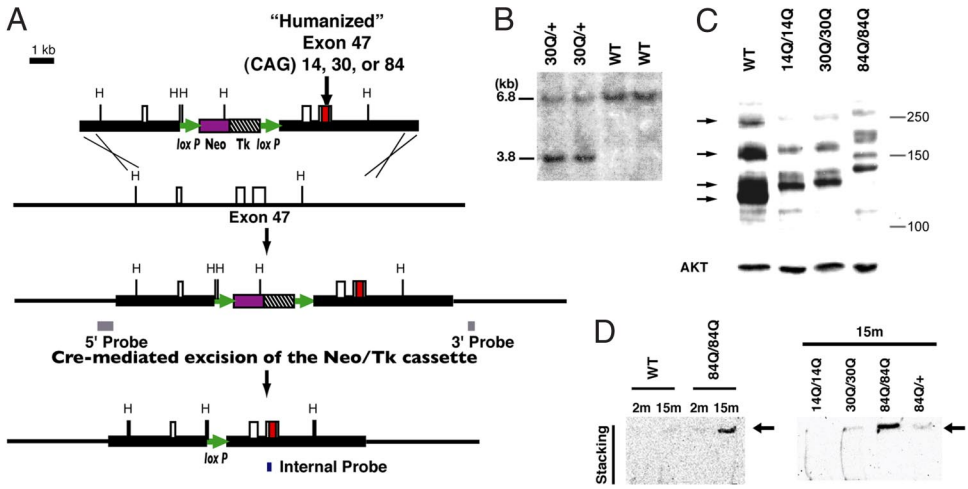

Fig. 1. Generation of Sca6 KI mice. (*A*) Targeting scheme represents the targeting construct, the endogenous *Sca6* allele, and the predicted structure of the mutant *Sca6* allele generated by a homologous recombination and a *Cre*-mediated excision event. (*B*) Germ-line transmission of a $Sca6^{30Q}$ allele. Southern blot analysis of HindIII-digested tail DNA revealed 6.8-kb WT and 3.8-kb mutant bands in $Sca6^{30Q/30Q}$ mice with the internal probe shown in *A*. (*C*) Western blot analysis performed on cytoplasmic fraction of cerebellar lysates from 6-month-old $Sca6^{14Q/14Q}$, $Sca6^{30Q/30Q}$, and $Sca6^{84Q/84Q}$ KI mice and a 6-month-old WT mouse, all blotted against CT-2 (*Upper*) and AKT (*Lower*, used as a loading control). Arrows indicate multiple CT-2 positive IRs detected with WT cerebellar lysates. Mutant $Ca_V2.1$ shows less mobility because of the polyglutamine stretch and its flanking human-specific sequence. (*D*) Detection of aggregated $Ca_V2.1$ channel in $Sca6^{84Q}$ cerebella. Shown are immunoblots of cerebellar extracts from 2- (2m) or 15-month-old (15m) $Sca6^{14Q/14Q}$ (14Q/14Q), $Sca6^{300Q/30Q}$, $Sca6^{84Q/+}$, $Sca6^{840Q/84Q}$ KI, and WT mice. Arrow indicates CT-2 IRs detected in the stacking part of the gels. Molecular masses are indicated at the right of each panel in kDa.

We next verified the presence of the GGCAG insertion in the KI alleles; this insertion is seen only in the MPI isoform and will ensure translation of the polyglutamine tract. cDNAs derived from laser-microdissected PCs were amplified and subcloned into plasmids. The splice variants were then identified by sequencing each individual clone. In this manner we confirmed the presence of all of the three splice variants in adult homozygous KI cerebella (Fig. S2*B*). Semiquantitative analysis of these variants revealed that the MPI isoform was most abundant in wild-type (WT) mice (Table 1). In all three lines of *Sca6* KI mice, however, the MPc isoform was the most abundant. Thus, the KI mutations led to reduced relative expression of the MPI isoform. Interestingly, in the PC layer of homozygous KI mice, the ratio of MPI copies to total isoform copies increased as a function of repeat length. These results suggest that the CAG repeat length also affected the patterns of splice events occurring at the boundary of exons 46 and 47 in mutant PCs.

The expression of WT and mutant $Ca_V2.1$ was assessed by immunoblotting with CT-2 antibody (Ab) (13). This Ab should react with the cytoplasmic C-terminal tail domain of the channel translated by MPI (Fig. S1*D*). With the cytoplasmic fraction of WT extracts, CT-2 demonstrated at least four immunoreactive bands with apparent molecular masses ranging from ≈120 kDa to >250 kDa (Fig. 1*C*). This pattern appeared to be similar to the immunoreactivities (IRs) recognized by anti-CT-1 Ab, which reacts with a highly conserved epitope located immediately adjacent to the polyglutamine tract (10), suggesting that these bands probably correspond to multiple $Ca_V2.1$ isoforms generated through alternative splicing. Mutant $Ca_V2.1$ is predicted to migrate less than WT $Ca_V2.1$, given the size of polyglutamine tract and its immediate human-specific sequence. As expected, cerebellar extracts from the homozygous KI mice gave multiple CT-2 IRs with less mobility on the gel as the repeat size became greater. Notably, extracts of the mutants gave less intense CT-2 IRs compared with WT extracts, consistent with the reduced MPI/MPc ratio in the homozygous KI cerebella. We also looked for the presence of polyglutamine-containing $Ca_V2.1$ C-terminal fragments showing apparent molecular masses <100 kDa. Such fragments were reported to be abundant in nuclei of cells overexpressing full-length $Ca_V2.1$ subunits (13). However, as shown in Fig. S2*C*, we could not detect such fragments because none of the CT-2 IRs, including those enriched in the nuclear fraction, revealed repeat-length-dependent C-terminal fragments on the blot.

We also examined whether aggregated mutant $Ca_V2.1$ subunits could be detected by immunoblotting with brain extracts prepared with urea/SDS-containing buffer. Cerebellar extracts from 15-month-old $Sca6^{84Q/84Q}$ KI mice gave CT-2 IR in the top part of the stacking gel, but this was not the case for their WT littermates nor for 2-month-old $Sca6^{84Q/84Q}$ KI mice (Fig. 1*D*). Those from 15-month-old $Sca6^{84Q/+}$ KI mice and 15-month-old $Sca6^{30Q/30Q}$ KI mice gave fainter CT-2 IR compared with 15-month-old $Sca6^{84Q/84Q}$ KI mice. These results suggest that the mutant $Ca_V2.1$ subunits containing an expanded polyglutamine tract formed insoluble aggregates in the cerebellum in an age- and gene dosage-dependent manner.

Table 1. Semiquantitative analysis of alternative splicing at exon 46/47 junction

Genotype	Variants, %			No. clones	No. animals
	MPI	MPc	MPII		
Wild type	55.6	44.4	0	55	3
$Sca6^{14Q/14Q}$	10.9	80.0	9.1	55	4
$Sca6^{30Q/30Q}$	19.4	77.4	3.2	31	2
$Sca6^{84Q/84Q}$	30.8	69.2	0	52	3

Phenotypic Analysis of *Sca6* KI Mice. By visual inspection, both heterozygous and homozygous $Sca6^{14Q}$, $Sca6^{30Q}$, and $Sca6^{84Q}$ KI mice were indistinguishable from their WT littermates up to 15 months of age. At 17 months of age, homozygous $Sca6^{84Q/84Q}$ mice of 129/SvEv background started to exhibit hypoactivity and less kempt fur compared with WT mice. As they aged further, the $Sca6^{84Q/84Q}$ mice exhibited these features even more clearly. Heterozygous $Sca6^{84Q/+}$, $Sca6^{30Q/30Q}$, and $Sca6^{30Q/+}$ mice were indistinguishable from WT littermates even after 20 months of age.

To assess motor impairment, WT and *Sca6* mutant mice were tested on the accelerating Rotarod at several time points (Fig. 2). We first tested F1 heterozygous $Sca6^{30Q/+}$ and $Sca6^{84Q/+}$ mice of C57BL/6J-129/SvEv background. The $Sca6^{30Q/+}$ mice performed similarly to WT littermates at 4, 11, and 19 months of age (Fig. 2*D* and data not shown). The $Sca6^{84Q/+}$ mice were tested at 4, 7, 11, and 19 months of age, and they performed as well as their WT littermates up to 11 months of age (data not shown). At 19 months of age, however, the performance of $Sca6^{84Q/+}$ mice became significantly worse than WT mice (Fig. 2*C*; $P < 0.01$), consistent with the $Sca6^{84Q}$ allele acting in a dominant fashion to induce age-dependent motor impairment.

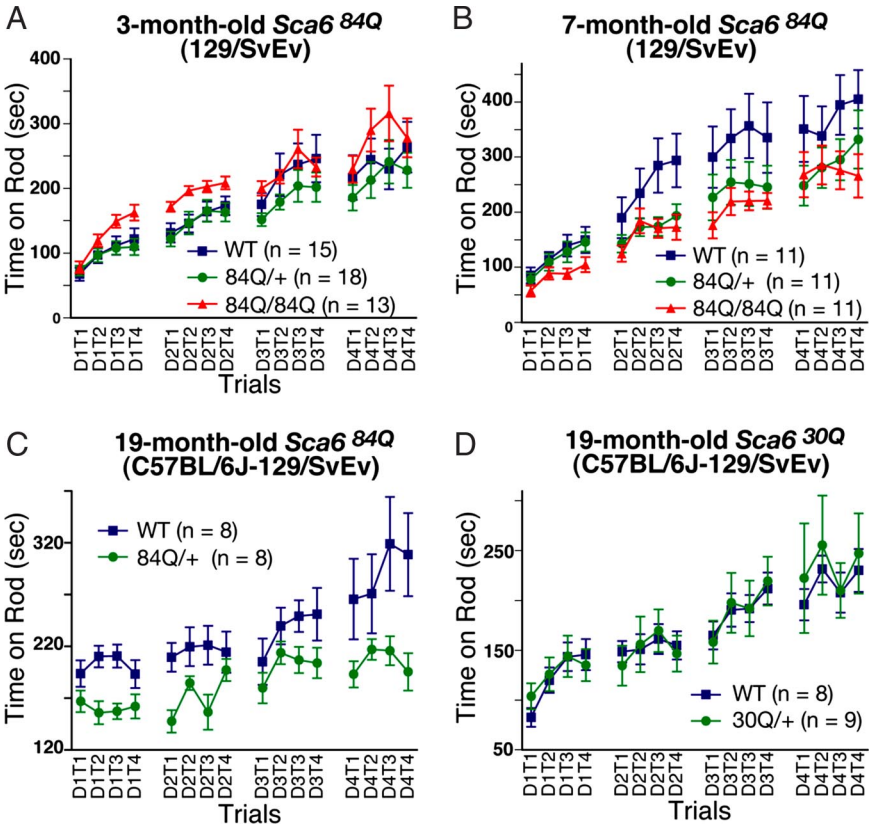

Fig. 2. Analysis of the *Sca6* KI mice on the accelerating Rotarod apparatus. (*A* and *B*) Performance of 3- (*A*) and 7- month-old (*B*) $Sca6^{84Q/84Q}$ mice of 129/SvEv background. $Sca6^{84Q/84Q}$ showed impaired motor performance ($P = 0.035$) at 7 months of age. (*C*) Performance of 19-month-old heterozygous $Sca6^{84Q/+}$ mice of C57BL/6J-129/SvEv background. (*D*) Performance of 19-month-old heterozygous $Sca6^{30Q/+}$ mice of C57BL/6J-129/SvEv background. Mice were trained in four trials per day (T1–T4) for four days (D1–D4). Error bars indicate SEM.

$Sca6^{84Q/84Q}$ mice of 129/SvEv pure background performed similarly to WT littermates at 3 months of age (Fig. 2*A*). By 7 months, however, the mutant mice performed worse than WT, staying on the Rotarod significantly less time (Fig. 2*B*; $P < 0.05$). At this same age, heterozygous $Sca6^{84Q/+}$ mice performed similarly to WT littermates ($P = 0.151$), consistent with our previous results (see above). In contrast to the $Sca6^{84Q/84Q}$ mice, neither the $Sca6^{30Q/30Q}$ nor $Sca6^{14Q/14Q}$ mice displayed impaired performance on the Rotarod by 7 months of age (Fig. S3). Taken together, our results demonstrate that only mice bearing the $Sca6^{84Q}$ allele develop motor impairment and that both the onset and severity of symptoms are gene dosage-dependent.

Properties of Ca^{2+} Channel Currents in Acutely Dissociated Cerebellar SCA6 PCs. To test the properties of SCA6 mutant channels *in vivo*, we recorded whole-cell Ca^{2+} channel currents in acutely dissociated PCs. Fig. 3 summarizes the results obtained recording WT and *Sca6* currents from PCs isolated from P12–P14 mice, using 2 mM Ba^{2+} as the charge carrier. Consistent with previous reports (14), the majority of inward current was blocked by 500 nM Aga-IVA, a specific peptide blocker of P/Q-type calcium channels; this was true for both WT and $Sca6^{84Q/84Q}$ neurons (Fig. 3 *A* and *B*). Although both groups of neurons contained similar Aga-IVA-insensitive components, the P/Q component was greatly decreased for the $Sca6^{84Q/84Q}$ neurons. Because the Aga-IVA-insensitive component is a minor contributor to whole-cell barium current density, subsequent experiments were conducted in the absence of blocker.

We next examined the *I–V* relationship of barium currents in WT and $Sca6^{84Q/84Q}$ neurons. In both groups, currents first became detectable with depolarization to −50 mV, peaked at −20 mV, and reversed at +30 mV (Fig. 3 *C* and *D*). Over a wide range of voltages, current density was significantly decreased in $Sca6^{84Q/84Q}$ (Fig. 3*C*), suggesting a voltage-independent effect.

To test whether the reduced current density seen in $Sca6^{84Q/84Q}$ neurons depends on CAG repeat length, we measured whole-cell current density in $Sca6^{14Q/14Q}$ and $Sca6^{30Q/30Q}$ PCs. Fig. 3*E* shows that all three polyglutamine-containing channels, irrespective of repeat length, exhibited a similar reduction in peak whole-cell current density relative to WT, suggesting that the decreased current does not depend on pathological expansion of the polyglutamine tract. Moreover, the reduced current density was not the result of increased cell size because whole-cell capacitance (a measure of plasma membrane surface area, and thus cell size) did not differ significantly among WT and the three groups of *Sca6* neurons (Fig. 3*F*).

Finally, we studied the effect of the long CAG repeat expansion on the voltage dependence of activation and inactivation, by using the protocols shown in Fig. 4 *A* and *B*, respectively. Neither activation, as measured by the *G–V* relationship, nor steady-state inactivation was significantly different between WT and $Sca6^{84Q/84Q}$ neurons (Fig. 4*C*).

Decreased $Ca_V2.1$ Immunoreactivity in $Sca6^{84Q/84Q}$ Purkinje Neurons. The decreased whole-cell current density observed in $Sca6^{84Q/84Q}$ PCs could be explained by either impaired channel function at the plasma membrane, as reported for a mutation associated with familial hemiplegic migraine type 1 (15), or a decrease in expression or protein stability. To test these possibilities, we used immunocytochemistry to measure total expression of $Ca_V2.1$ in acutely dissociated PCs. Fig. S4*A* shows typical examples of a WT and an $Sca6^{84Q/84Q}$ PC, identified by morphology and selective staining for type III β-tubulin using the Tuj1 Ab. The $Ca_V2.1$ protein was immunostained with an Ab raised against the intracellular linker between domains II and III (the II–III loop). Consistent with our whole-cell capacitance measurements (Fig. 3*F*), cell cross-sectional area (measured with the β-tubulin immunofluorescence) was not significantly different between WT and $Sca6^{84Q/84Q}$. In contrast, $Ca_V2.1$ immunofluorescence was significantly decreased for $Sca6^{84Q/84Q}$ PCs (Fig. S4*B*). The degree of reduction in $Ca_V2.1$ immunofluorescence nearly paralleled the degree of reduction in

NEUROSCIENCE

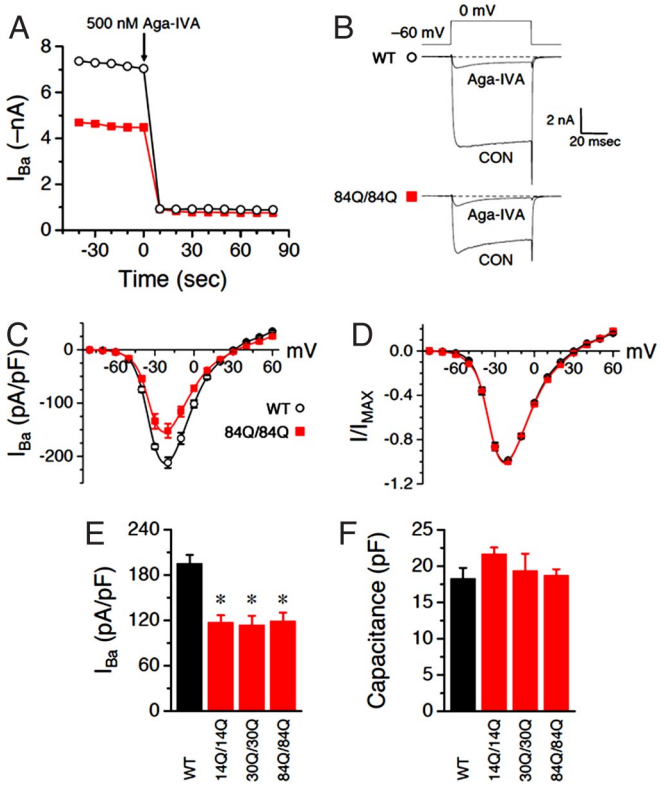

Fig. 3. Whole-cell Purkinje Ba^{2+} currents are blocked by Aga-IVA and reduced in *Sca6* neurons. (*A*) Time course of peak current for a WT (○) or an $Sca6^{84Q/84Q}$ (■) neuron. Aga-IVA was added to the bath when indicated, to a final bath concentration of ≈500 nM. (*B*) Individual traces from the two cells in *A*, before and after bath application of Aga-IVA. (*C–F*) Each group consists of 4–19 neurons. (*C*) Current density was plotted against voltage for WT (○) and $Sca6^{84Q/84Q}$ (■) neurons. (*D*) Same data as in *A*, normalized to peak inward current. (*E*) Summary of whole-cell current density at −15 mV. *, $P < 0.005$ vs. WT (by two-tailed Student's unpaired *t* test). (*F*) Summary of whole-cell capacitance. $P > 0.05$ vs. WT for all three *Sca6* populations. 14Q/14Q, 30Q/30Q, and 84Q/84Q represent $Sca6^{14Q/14Q}$, $Sca6^{30Q/30Q}$, and $Sca6^{84Q/84Q}$, respectively.

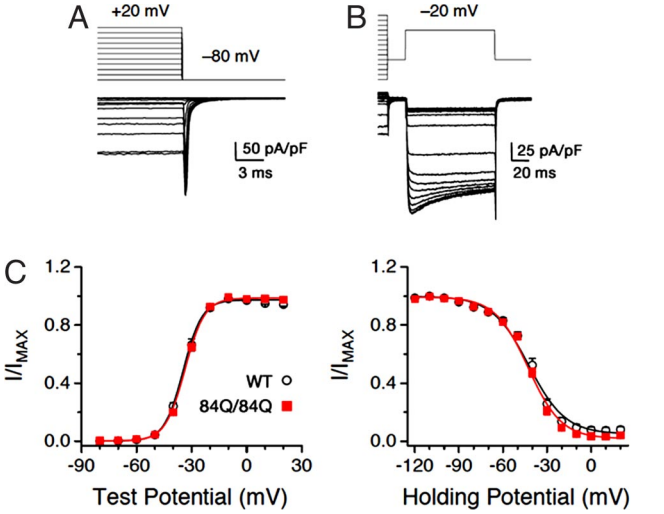

Fig. 4. Sca6 mutations do not affect activation or inactivation. (*A*) Protocol used to measure activation (*G–V*) curves. Shown are currents from a WT PC. The cell was held at −80 mV and depolarized for 60 ms to incremental voltages from −80 through +20 mV. Peak tail current amplitude was normalized and plotted against voltage to generate the curves in *C*. (Scale bars: vertical, 50 pA/pF; horizontal, 3 ms.) (*B*) Protocol used to measure steady-state inactivation for the same cell shown in *A*. The cell was held at −80 mV, and a 3-s conditioning pulse was applied in 10-mV increments from −120 through +20 mV followed by a test pulse to −20 mV. Peak current amplitude during the test pulse was normalized and plotted against conditioning pulse voltage to generate the curves in *C*. (*C*) Summary of activation and inactivation curves for WT (○) and $Sca6^{84Q/84Q}$ (■) PCs. Solid lines are Boltzmann fits of the data. For activation, WT and $Sca6^{84Q/84Q}$ $V_{0.5}$ are −34.0 ± 0.9 and −33.1 ± 0.5 mV, respectively ($P > 0.4$, by two-tailed Student's unpaired *t* test); slope factors (*k*) are 4.8 ± 0.2 and 4.8 ± 0.1, respectively ($P > 0.9$). For inactivation, WT and $Sca6^{84Q/84Q}$ $V_{0.5}$ are −41.8 ± 1.0 and −41.6 ± 0.8 mV, respectively ($P > 0.8$); slope factors (*k*) are 10.0 ± 0.7 and 9.3 ± 0.5, respectively ($P > 0.4$). $n = 10–13$ neurons.

peak whole-cell current density, suggesting that decreased whole-cell current density could mainly be attributed to decreased $Ca_V2.1$ channel abundance.

Neuropathology of $Sca6^{84Q/84Q}$ Brains. To assess possible neuropathological changes, we compared brain sections from $Sca6^{84Q/84Q}$ mice with those from WT mice. Hematoxylin/eosin and cresyl violet stains revealed no gliosis or neuronal loss in the brains of $Sca6^{84Q/84Q}$ mice up to 20 months of age (data not shown), an age at which motor deficits were evident.

We next asked whether the *Sca6* mutation resulted in neuropathological changes in PCs through either loss- or gain-of-function mechanism. PCs in $Ca_V2.1$ knockout mice have been reported to display altered cytological differentiation such as hyperspiny transformation of PC dendrites and soma and a decrease of dendritic innervation by climbing fibers (CFs) (16). Accordingly, we investigated the morphology of PCs and the distribution patterns of CF terminals in $Sca6^{84Q/84Q}$ mice at 24 months of age by using Abs against calbindin and VGluT2, respectively. In double immunofluorescence for calbindin (Fig. S5 *A* and *C*, green) and VGluT2 (Fig. S5 *A–D*, red), there were no clear differences between WT and $Sca6^{84Q/84Q}$ mice. The soma and proximal dendrites of PCs had a smooth surface in both mice (Fig. S5 *A* and *C*). VGluT2-positive terminals were distributed along thick proximal dendrites within four-fifths of the molecular layer in both mice (Fig. S5 *A–D*). We also found no differences in the distribution patterns of parallel fiber or inhibitory terminals as demonstrated by immunofluorescence for VGluT1 (Fig. S5 *E* and *G*) or VGAT (Fig. S5 *F* and *H*), respectively. Therefore, the morphology of PCs and distribution pattern of CF terminals were not altered in $Sca6^{84Q/84Q}$ mice. We also performed semiquantitative analysis of calbindin immunofluorescence on cerebellar sections (17) to detect subtle dendritic degeneration. This analysis did not reveal any alterations in calbindin immunofluorescence in the molecular layer of $Sca6^{84Q/84Q}$ cerebella up to 22 months of age (data not shown).

To assess the subcellular distribution of the $Ca_V2.1$ channel bearing the long cytoplasmic tail domain, we performed immunohistochemical analysis with an affinity-purified, antipeptide, $Ca_V2.1$ Ab (named A6RPT-polyQ). This Ab was raised against the epitope specifically expressed in the C-terminal part of the human $Ca_V2.1$ subunit and should not react with WT mouse $Ca_V2.1$ channel (Fig. S1*D*). In the cerebella of 22-month-old $Sca6^{84Q/84Q}$ mice, we detected neuronal inclusions (NIs) predominantly in the cytoplasm of scattered PCs (Fig. 5*A*). No such NI formation was ever detected in WT or $Sca6^{14Q/14Q}$ mouse brains of the same age (Fig. 5*B*). These results suggest that aged $Sca6^{84Q/84Q}$ mice developed neuronal inclusions, which were reminiscent of those seen in human SCA6 PCs (18, 19), without apparent neurodegenerative changes.

Discussion

The three lines of *Sca6* mice generated in this work demonstrate repeat length- and dosage-dependent motor deficits like those seen in SCA6 patients. SCA6 patients with 30 repeats typically do not manifest symptoms until their 40s or 50s. Thus, it is not surprising that, as in other polyglutamine KI models, only hyperexpanded *Sca6* alleles (not seen in adult-onset SCA6 patients) manifest a

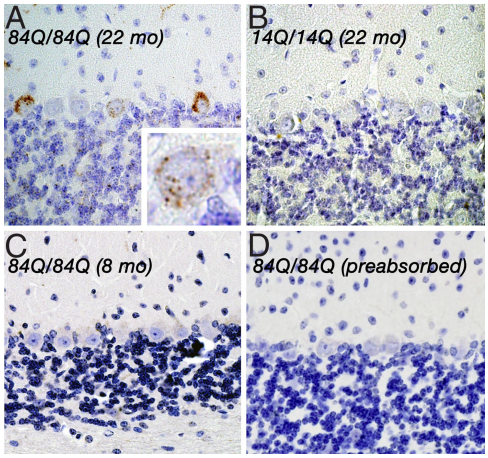

Fig. 5. NI formation in *Sca6*$^{84Q/84Q}$ Purkinje neurons. (*A*) Immunohistochemistry for A6RPT-polyQ revealed NI formation in *Sca6*$^{84Q/84Q}$ PCs (22-month-old). (*Inset*) Individual PC at higher magnification. Note that these NIs were seen mainly in the cytoplasm of these neurons. Similar NI-harboring PCs were scattered in the cerebellum. (*B* and *C*) In contrast, only weak immunoreactivities were detected in the cerebellum of a 22-month-old *Sca6*$^{14Q/14Q}$ (*B*) or an 8-month-old *Sca6*$^{84Q/84Q}$ mouse (*C*). (*D*) The immunoreactivity was entirely blocked in the cerebellum of the 22-month-old *Sca6*$^{84Q/84Q}$ mouse when A6RPT-polyQ was preincubated with its polypeptide antigens. (Magnification of original photographs, ×400.) Parallel staining undertaken with control human specimen also revealed similar NI formation in SCA6 PCs (data not shown).

phenotype in the relatively short life span of the mouse (17, 20–22). The absence of motor phenotype in heterozygous or homozygous *Sca6*^{30Q} mice also appears to support the notion that SCA6 is not a simple channelopathy because previously described loss-of-function *Cacna1a* mutants often show early-onset motor phenotypes associated with distinct alterations of Ca^{2+} channel properties (23, 24).

One critical genetic feature of SCA6 is that the mutation is located in exon 47, where alternative splicing produces two major isoforms, MPI and MPc. Our data revealed a reduced MPI/MPc ratio in Purkinje cell layers of the cerebella of all KI alleles. We speculate that the single *lox*P sequence left in the intron and/or the human nucleotide sequence in chimeric exon 47 contributed to the altered splice patterns at this locus. It is interesting, however, that the relative abundance of MPI transcripts increased as the CAG repeat length increased. This finding is in good agreement with the observation that the cerebellar transcripts containing 28 CAG repeats, obtained from the cerebellar cortex of an SCA6 patient, had a higher relative abundance of the GGCAG-containing variant compared with those containing 13 CAG repeats (18). It is not clear how CAG repeat length affects splicing, but we propose that the CAG repeat itself or its flanking sequence may act as an exonic *cis*-element contributing to correct splice-site identification. Indeed, online searches through ESEfinder (25) predicted the location of several putative exonic splicing enhancer motifs that include part of the CAG repeat (data not shown). Expansion of the repeat may alter the binding of specific serine/arginine-rich proteins to the motif(s) and thereby influence the splicing patterns at this locus.

Whether SCA6 arises from direct alteration of the channel function or a cytotoxic gain-of-function effect caused by the polyglutamine stretch has been a hotly debated topic (26). Our Sca6 KI animals gave us an opportunity to assess the effect of the SCA6 mutation on the function of voltage-gated calcium channels in PCs. Contrary to the previous reports (8–11), our results clearly indicate that the hyperexpanded *Sca6*^{84Q} mutation does not alter voltage sensitivity of activation or inactivation in the acutely dissociated PCs. The *Sca6*$^{84Q/84Q}$ PCs showed reduced $Ca_V2.1$ immunoreactivity and a corresponding reduction of whole-cell current density compared with WT PCs. However, this reduction was not caused by repeat length because a similar reduction was observed for both the *Sca6*$^{14Q/14Q}$ and *Sca6*$^{30Q/30Q}$ channels, suggesting that the reduced current density seen in the *Sca6*$^{84Q/84Q}$ PCs is not the key factor that accounts for the neurological phenotypes unique to these animals. Saegusa *et al.* (27) recently reported KI mice expressing a cDNA encoding a single MPI isoform of the human $Ca_V2.1$ channel. Electrophysiological analysis on their homozygous mutants also indicated that the repeat length did not affect the basic properties of the channel, although the expression levels of the human $Ca_V2.1$ channel were greatly reduced in these mice.

Decreased protein turnover and aggregation are common features of polyglutamine diseases, and accumulation of the polyglutamine-containing protein is thought to underlie a toxic gain-of-function mechanism (4). Thus, our observations that the mutant $Ca_V2.1$ channel did not lose its function and that its aggregation occurred in *Sca6*^{84Q} cerebella in both an age- and dosage-dependent manner support the notion that SCA6 is caused by a toxic gain-of-function mechanism. At least two forms of $Ca_V2.1$ accumulation (surface and cytoplasmic) have been implicated in the SCA6 pathogenesis (11, 18, 19). Although the Ab used here showed cytoplasmic mutant $Ca_V2.1$ aggregation in cerebellar PCs of *Sca6* $^{84Q/84Q}$ mice, further study using mice with larger expanded alleles will be necessary to determine whether the mutant $Ca_V2.1$ also accumulates on the cellular surface or in the presynaptic terminals over time and ultimately changes the Ca^{2+} homeostasis in PCs of aged mutant mice. Such accumulation could lead to altered synaptic neurotransmission like that seen in flies expressing expanded full-length htt (28) and thereby induce motor dysfunction before the appearance of detectable neurodegeneration.

Kordasiewicz *et al.* (13) have found that the C-terminal region of $Ca_V2.1$ is capable of being cleaved from the protein, translocating to the nucleus, and causing toxicity to cells if it contained an expanded polyglutamine tract. Kubodera *et al.* (29) also reported the production of similar fragment in HEK293T cells overexpressing $Ca_V2.1$. Interestingly, the C terminus of the L-type $Ca_V1.2$ Ca^{2+} channel can also be cleaved and translocate to the nucleus, where it may act as a transcription factor (30). In our *Sca6* KI mice, we could not detect such a small C-terminal fragment in cerebellar extracts. It is conceivable that the cleaved product is sequestered with the large aggregated channel. Alternatively, the polyglutamine-containing cleavage product may be produced only when $Ca_V2.1$ is overexpressed in the heterologous context. Finally, it is possible that chimeric $Ca_V2.1$ protein produced in the KI brains may be no longer susceptible to such processing. Irrespective of the reason for the lack of aberrant accumulation of the cleaved product, it seems that such an event is not necessary to cause the neurological impairment seen in *Sca6*$^{84Q/84Q}$ mice.

In conclusion, introducing the expanded CAG tract into $Ca_V2.1$ did not alter the basic properties of P/Q-type calcium channels but led to motor impairment coupled with aggregation of mutant $Ca_V2.1$. Both occurred in a dosage- and age-dependent manner as typically found in human SCA6. Also similar to human SCA6, increasing CAG repeat length increased the proportion of MPI transcripts in the cerebellum. Thus, the *Sca6* mutation not only gives rise to transcripts encoding glutamine-expanded channel proteins but also up-regulates their expression, possibly by regulating splicing events. We hypothesize that SCA6 pathogenesis must involve a toxic gain-of-function mechanism caused by altered activities or interactions of the C-terminal fragment in addition to possible partial loss-of-function due to decreased levels of specific isoforms.

Materials and Methods

Further details are described in *SI Materials and Methods*.

Generation of Sca6 KI Mice. Clones obtained from the 129/SvEv mouse genomic DNA library were used to construct a targeting vector. A SacII fragment that includes part of the mouse *Sca6* exon 47 was replaced with the homologous fragment prepared from human $Ca_V2.1$ cDNAs (12). A selectable cassette containing the neomycin resistance gene (*Neo*) and the thymidine kinase gene (*Tk*) flanked by two *lox*P sites were inserted into intron 45. The 72 CAG repeats were expanded to 84 during the ligation steps. The resultant targeting constructs were electroporated into ES cells derived from 129/SvEv strain, and subsequent electroporation of Cre recombinase expressing plasmids allowed the excision of *Neo*/*Tk* selection cassette. Correctly targeted ES cells were injected into C57BL/6J blastocysts to generate chimeras.

Laser Microdissection. Sagittal cerebellar tissue cryosections 8 μm in thickness were mounted on polyethylene membrane slides (Leica). Each cryosection was lightly fixed in 95% ethanol and 5% acetic acid followed by a brief rinse in ice-cold water before staining with HistoGene staining solution (Arcturus). Laser microdissection was performed by using an AS LMD system (Leica). Total RNA from these samples was extracted by using the RNeasy micro kit following the manufacturer's instructions. The quality of RNA was checked with RNA 6000 Pico LabChip Kit (Agilent).

Semiquantitative RT-PCR. The reverse-transcription reaction was carried out with Sensiscript reverse transcriptase (Qiagen) following the manufacturer's instructions.

Primers MuEx46F3 (5′-AAGCATCGGCCACACCACCACCACCA-3′) and TAARev (5′- TTAGCACCAGTCGTCCTCGCTCTCGCTGTAC-3′) were used to amplify the part of the cDNA containing both the junction of exon 46/47 and the CAG repeat.

Amplified products were cloned into pCRII-TOPO vector (Invitrogen). Clones were picked up for each RNA sample and subjected to sequencing.

Protein Expression. Protein extracts of mouse cerebellum were obtained by using NE-PER nuclear and cytoplasmic extraction reagents (Pierce). Fifty micrograms of protein was loaded on SDS gel. For detection of aggregated forms of $Ca_V2.1$, samples were lysed in buffer containing 8 M urea and 4% SDS. Nitrocellulose blots were probed with CT-2 Ab (1:1,000).

Rotarod Test. Animals were placed on an accelerated rotating rod (Ugo Basile) in four trials every day for a period of 4 days, as described in ref. 31.

PC Preparation. Neurons were prepared from P12–P14 cerebella with a protocol modified from Swensen and Bean (32). The cells were plated on coverslips precoated with poly-D-lysine and laminin (BD Biosciences) in a 24-well plate containing Neurobasal complete medium (containing sodium pyruvate, L-glutamine, B27, and *N*-acetylcysteine).

Electrophysiology. Whole-cell currents were recorded at room temperature by using an Axopatch 200B patch-clamp amplifier (Axon Instruments). Pipette resistance was ≈2–3 MΩ when filled with an internal solution. Cells were voltage-clamped at −80 mV, and pulse depolarizations were applied at 10-s intervals. Data were passed through a 4-pole low-pass Bessel filter at 1–2 kHz, digitized at 5–10 kHz by using a Digidata 1320A (Axon Instruments). Patch-clamp data were acquired and analyzed by using Clampex 8.2 and Clampfit 8.2, respectively (Molecular Devices).

Immunohistochemistry. Formalin-fixed, paraffin-embedded, 6-μm-thick sections were deparaffinized, exposed to microwave in citrate buffer, and treated in formic acid before incubation with human $Ca_V2.1$-specific custom Abs A6RPT-polyQ raised against MERRVPGPARSESPRA (Fig. S1*D*). Detailed characterization of the Abs will be published elsewhere.

Statistical Analysis. Where applicable, data are presented as mean ± SEM, and statistical significance was tested by using a two-tailed Student's unpaired *t* test for the electrophysiological analysis and semiquantitative measurements of $Ca_V2.1$ immunofluorescence. For the Rotarod test, the time the mice spent on the rod without falling was recorded and subjected to statistical analysis by using one-way ANOVA with repeated measures.

ACKNOWLEDGMENTS. We thank Andy Swensen for helpful advice on Purkinje cell preparation; Barbara Antalffy, Richard Atkinson, and Gabriele Schuster for technical support; and Cheng Chi Lee (University of Texas, Houston) and Olga Zhuchenko (Baylor College of Medicine) for the generous gift of human $Ca_V2.1$ cDNAs. This work was supported by Ministry of Education, Science, and Culture of Japan Grant 17209031 (to H.M.), National Institute of Neurological Disorders and Stroke/National Institutes of Health Grant NS24607 (to R.W.T.), and by a private foundation that has asked that its identity not be disclosed (to H.Y.Z.). H.Y.Z. is an investigator and K.W. is a research associate with the Howard Hughes Medical Institute.

1. Zhuchenko O, *et al.* (1997) Autosomal dominant cerebellar ataxia (SCA6) associated with small polyglutamine expansions in the α1A-voltage dependent calcium channel. *Nat Genet* 15:62–69.
2. Ishikawa K, *et al.* (1997) Japanese families with autosomal dominant pure cerebellar ataxia map to chromosome 19p13.1-p13.2 and are strongly associated with mild CAG expansions in the spinocerebellar ataxia type 6 gene in chromosome19p13.1. *Am J Hum Genet* 61:336–346.
3. Tsuchiya K, *et al.* (2005) Degeneration of the inferior olive in spinocerebellar ataxia 6 may depend on disease duration: Report of two autopsy cases and statistical analysis of autopsy cases reported to date. *Neuropathology* 25:125–135.
4. Gatchel JR, Zoghbi HY (2005) Diseases of unstable repeat expansion: Mechanisms and common principles. *Nat Rev Genet* 6:743–755.
5. Mariotti C, *et al.* (2001) Pathogenic effect of an intermediate-size SCA6-allele (CAG)(19) in a homozygous patient. *Neurology* 57:1502–1504.
6. Mintz IM, Sabatini BL, Regehr WG (1995) Calcium control of transmitter release at a cerebellar synapse. *Neuron* 15:675–688.
7. Walker JT, Alvina K, Womack MD, Chevez C, Khodakhah K (2006) Decrease in the precision of Purkinje cell pacemaking causes cerebellar dysfunction and ataxia. *Nat Neurosci* 9:389–397.
8. Matsuyama Z, *et al.* (1999) Direct alteration of the P/Q-type Ca^{2+} channel property by polyglutamine expansion in spinocerebellar ataxia 6. *J Neurosci* 19: RC14.
9. Toru S, *et al.* (2000) Spinocerebellar ataxia type 6 mutation alters P-type calcium channel function. *J Biol Chem* 275:10893–10898.
10. Restituito S, *et al.* (2000) The polyglutamine expansion in spinocerebellar ataxia type 6 causes a β subunit-specific enhanced activation of P/Q type calcium channels in *Xenopus* oocytes. *J Neurosci* 20:6394–6403.
11. Piedras-Renteria ES, *et al.* (2001) Increased expression of α1A Ca^{2+} channel currents arising from expanded trinucleotide repeats in spinocerebellar ataxia type 6. *J Neurosci* 21:9185–9193.
12. Tsunemi T, *et al.* (2002) Novel Cav2.1 splice variants isolated from Purkinje cells do not generate P-type Ca^{2+} current. *J Biol Chem* 277:7214–7221.
13. Kordasiewicz HB, Thompson RM, Clark HB, Gomez CM (2006) C termini of P/Q-type Ca^{2+} channel α1A subunits translocate to nuclei and promote polyglutamine-mediated toxicity. *Hum Mol Genet* 15:1587–1599.
14. Ramen IM, Bean BP (1999) Ionic currents underlying spontaneous action potentials in isolated cerebellar Purkinje neurons. *J Neurosci* 19:1663–1674.
15. Barrett CF, Cao Y-Q, Tsien RW (2005) Gating deficiency in a familial hemiplegic migraine type 1 mutant P/Q-type calcium channel. *J Biol Chem* 280:24064–24071.
16. Miyazaki T, Hashimoto K, Shin H-S, Kano M, Watanabe M (2004) P/Q-type Ca^{2+} channel α1A regulates synaptic competition on developing cerebellar Purkinje cells. *J Neurosci* 24:1734–1743.
17. Watase K, *et al.* (2002) A long CAG repeat in the mouse Scal locus replicates SCA1 features and reveals the impact of protein solubility on selective neurodegeneration. *Neuron* 34:905–919.
18. Ishikawa K, *et al.* (1999) Abundant expression and cytoplasmic aggregations of α1A voltage-dependent calcium channel protein associated with neurodegeneration in spinocerebellar ataxia type 6. *Hum Mol Genet* 8:1185–1193.
19. Ishikawa K, *et al.* (2001) Cytoplasmic and nuclear polyglutamine aggregates in SCA6 Purkinje cells. *Neurology* 56:1753–1756.
20. Lin C-H, *et al.* (2001) Neurological abnormalities in a knockin mouse model of Huntington's disease. *Hum Mol Genet* 10:137–144.
21. Yoo S-Y, *et al.* (2003) SCA7 knockin mice model human SCA7 and reveal gradual accumulation of mutant ataxin-7 in neurons and abnormalities in short-term plasticity. *Neuron* 37:383–401.
22. Lorenzetti D, *et al.* (2000) Repeat instability and motor incoordination in mice with a targeted expanded CAG repeat in the Scal locus. *Hum Mol Genet* 9:779–785.
23. Dove LS, Abbott LC, Griffith WH (1998) Whole-cell and single-channel analysis of P-type calcium currents in cerebellar Purkinje cells of leaner mutant mice. *J Neurosci* 18:7687–7699.
24. Wakamori M, *et al.* (1998) Single tottering mutations responsible for the neuropathic phenotype of the P-type calcium channel. *J Biol Chem* 273:34857–34867.
25. Cartegni L, Wang J, Zhu Z, Zhang MQ, Krainer AR (2003) ESEfinder: A web resource to identify exonic splicing enhancers. *Nucleic Acids Res* 31:3568–3571.
26. Frontali M (2001) Spinocerebellar ataxia type 6: Channnelopathy or glutamine repeat disorder? *Brain Res Bull* 56:227–231.
27. Saegusa H, *et al.* (2007) Properties of human $Ca_V2.1$ channel with a spinocerebellar ataxia type 6 mutation in Purkinje cells. *Mol Cell Neurosci* 34:261–270.
28. Romero E, *et al.* (2008) Suppression of neurodegeneration and increased neurotransmission caused by expanded full-length Huntingtin accumulating in the cytoplasm. (2008) *Neuron* 57:27–40.
29. Kubodera T, *et al.* (2003) Proteolytic cleavage and cellular toxicity of the human α1A calcium channel in spinocerebellar ataxia type 6. *Neurosci Lett* 341:74–78.
30. Gomez-Ospina N, Tsuruta F, Barreto-Chang O, Dolmetsch R (2006) The C terminus of the L-type voltage-gated calcium channel Ca(V)1.2 encodes a transcription factor. *Cell* 127:591–606.
31. Watase K, *et al.* (2007) Lithium therapy improves neurological function and hippocampal dendritic arborization in a spinocerebellar ataxia type 1 mouse model. *PloS Med* 4:e182.
32. Swensen AM, Bean BP (2003) Ionic mechanisms of burst firing in dissociated Purkinje cells. *J Neurosci* 23:9650–9663.